Earth and Planetary Science Letters xxx (2010) xxx–xxx

Contents lists available at ScienceDirect

Earth and Planetary Science Letters

journal homepage: www.elsevier.com/locate/epsl

Reconciling patterns of interseismic strain accumulation with thermal observations across the Carrizo segment of the San Andreas Fault

Patrick M. Fulton [a,*], Gina Schmalzle [b], Robert N. Harris [a], Timothy Dixon [c]

[a] College of Oceanic and Atmospheric Sciences, Oregon State University, Corvallis, OR, USA
[b] Earth and Space Sciences, University of Washington, Seattle, WA, USA
[c] Rosenstiel School of Marine and Atmospheric Sciences, University of Miami, Miami, FL, USA

ARTICLE INFO

Article history:
Received 9 June 2010
Received in revised form 8 October 2010
Accepted 17 October 2010
Available online xxxx

Editor: R.D. van der Hilst

Keywords:
strain accumulation
geodesy
heat flow
overpressures
San Andreas Fault

ABSTRACT

The Carrizo segment of the San Andreas Fault separates rocks of the Salinian Block southwest of the fault characterized by high heat flow (~75–95 mW/m^2) and shallow seismicity (<~10 km depth), from rocks of the Franciscan Complex and Great Valley Group northeast of the fault associated with low heat flow (50–60 mW/m^2) and deeper seismicity (<~20 km depth). GPS data from this region suggest that the northeast side of the fault accommodates more interseismic strain than the southwest side. We show that by incorporating variations in depth to the brittle ductile transition inferred based on heat flow and seismicity data, we fit the geodetic data well and achieve agreement with geologically accepted long-term average slip rates with a ~20 km wide zone with low Young's modulus NE of the fault. This wide compliant zone is consistent with observations suggesting that the presence of large overpressures may be decreasing the elastic moduli in this region.

1. Introduction

Large faults can juxtapose terrains having considerable contrasts in physical, thermal, and hydrogeologic characteristics. These contrasts can have important implications for strain accommodation and may play an important role in the regional seismic hazard (e.g., Barbot et al., 2008; Ben-Zion and Huang, 2002; Schmalzle et al., 2006). Patterns of asymmetric interseismic strain accumulation have been observed in geodetic data across locked segments of mature, active strike-slip faults in numerous locations, including the Main Marmara Fault segment of the North Anatolian Fault Zone in Turkey (Le Pichon et al., 2003, 2005) and several segments of the San Andreas Fault Zone such as near Point Arena and Point Reyes in Northern California (Jolivet et al., 2009; Le Pichon et al., 2005; Prescott and Yu, 1986), the Carrizo Plain in Central California (Lisowski et al., 1991; Schmalzle et al., 2006), and across the Salton Sea in Southern California (Fay and Humphreys, 2005; Fialko, 2006; Lisowski et al., 1991). Processes leading to asymmetric interseismic strain accumulation are poorly understood, but are hypothesized to include laterally variable depths to the brittle ductile transition zone (Chéry, 2008; Schmalzle et al., 2006), non-vertical fault geometry (Fialko, 2006; Wei and Sandwell, 2008), laterally varying viscosity (Malservisi et al., 2001) or lateral variations in elastic modulus across the fault zone (Fialko, 2006; Le Pichon et al., 2005; Lisowski et al., 1991; Schmalzle et al., 2006). Because models of interseismic strain accumulation are inherently non-unique, understanding processes associated with asymmetric strain accumulation requires using as many independent datasets as possible. We show that heat flow and seismicity data provide independent constraints on model parameters and can aid in interpreting model results in terms of the underlying fault zone characteristics and processes that control interseismic strain accumulation.

In this study, we focus on the Carrizo segment of the San Andreas Fault (SAF) in central California. The Carrizo segment separates rocks of the Salinian Block, mostly composed of granites and granodiorites south of the fault, from rocks of the Franciscan Complex and Great Valley Group northeast of the fault. The Franciscan Complex is ~20 km wide and contains a sub-horizontal serpentine body associated with the Coast Range Ophiolite at depth that forms a low permeability hydrologic seal. The Great Valley sequence overlays the Franciscan and continues further to the northeast (Irwin, 1990; Page, 1981).

Along the Carrizo segment, the SAF consists of one major strand that is long and straight, supports strike-slip motion, and is locked during interseismic periods. Strike-slip motion in this region initiated ~22 Ma resulting in ~315 km of offset, with motion along the current primary strand of the fault for at least the past 5 Ma (Sims, 1993); thus, the SAF in this region is a mature fault and an ideal place to study the details of strain accommodation. GPS displacement rate data from

* Corresponding author. Now at Institute for Geophysics, University of Texas at Austin, Austin, TX, USA.
E-mail address: pfulton@ig.utexas.edu (P.M. Fulton).

0012-821X/$ – see front matter © 2010 Elsevier B.V. All rights reserved.
doi:10.1016/j.epsl.2010.10.024

this region reveal asymmetric strain accumulation across the fault showing that the northeast side of the fault accommodates more interseismic strain than the southwest side (Fig. 1) (Schmalzle et al., 2006). We find the observation of greater interseismic strain accumulation on the northeast side curious, because heat flow and seismicity data suggest that the northeast side of the fault has a considerably thicker elastic thickness than the southwest side (Fig. 2).

Schmalzle et al. (2006) tested two hypotheses regarding asymmetric strain accumulation in this region: that asymmetric strain is caused by 1) lateral variations in the depth of the brittle–ductile layer, or 2) lateral variations in Young's modulus within the elastic layer. In their study, each hypothesis was treated separately. In one model a low misfit was obtained using a constant Young's modulus and an elastic layer 10 km thick southwest of the fault and 8 km thick northeast of the fault. The base of the elastic layer was interpreted as the depth of the brittle–ductile transition. A second low misfit model consisted of a constant elastic thickness of 15 km, but included a 20 km wide compliant zone northeast of the fault to explain the asymmetry (Fig. 1).

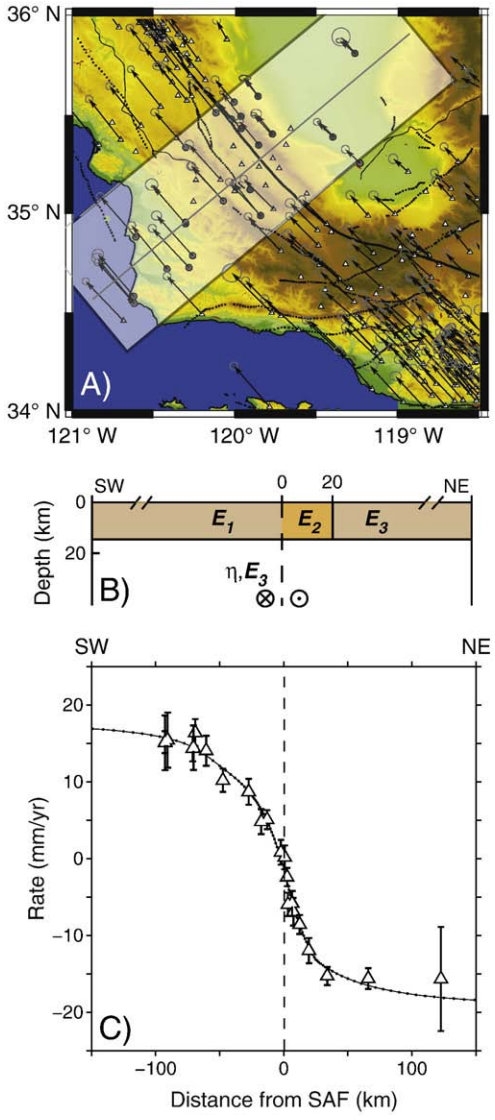

Fig. 1. A) Topographic map with GPS velocity vectors. GPS data used in this study are within the shaded box. Data are laterally projected along the transect line perpendicular to the San Andreas Fault and are shown in panel C along with the preferred viscoelastic halfspace model of Schmalzle et al. (2006) with a 20 km wide compliant zone in an uniformly thick elastic layer NE of the SAF, illustrated in panel B. After Schmalzle et al. (2006).

In this study, we update these models by constraining elastic layer thicknesses using heat flow and seismicity data and minimize the misfit by varying Young's modulus within the compliant zone along with the long-term slip rate. Heat flow and seismicity data along the Carrizo segment suggest a sharp contrast in the thermal regime across the fault (Fig. 2). The Salinian block southwest of the fault is characterized by high heat flow, with values of ~75–95 mW m^{-2}, while the Franciscan and Great Valley sequence to the northeast is characterized by low heat flow, with values of ~40–60 mW m^{-2}. Extrapolations of geotherms predict the 350 °C isotherm at depths of ~10 and ~20 km for the southwest and northeast sides of the fault, respectively. These depths correspond to the 90% cutoff depth in seismicity on each side of the fault (Fig. 2). We infer that the correlations between the 350 °C isotherm and the depth cutoff in seismicity mark the brittle–ductile transition and use these depths as elastic thicknesses in our viscoelastic numerical models.

2. Model setup

We use the finite element code G-TECTON version 1.3 (Govers, 1993; Melosh and Raefsky, 1980) to develop a suite of '2.5-dimensional' LaGrangian plane strain finite element models. In two dimensions, these models describe an elastic layer representing the brittle seismogenic crust that is coupled (i.e. welded) to a viscoelastic layer beneath (Fig. 3). The elastic layer contains a vertical strike slip fault that extends from the surface to the top of the viscoelastic layer and is defined using the split node technique (Melosh and Raefsky, 1981). Split nodes along the fault plane are displaced a defined amount at specified points in time. The model is referred to as "2.5-dimensional" because displacements are perpendicular to the 2-dimensional plane of the model; no displacement gradients occur in the out of plane direction. Constitutive equations are listed in Schmalzle et al. (2006).

The models extend 500 km laterally on either side of the fault and 500 km from the surface to reduce edge effects. Node density near the fault is increased to decrease mesh effects. The elastic layer thickness southwest of the SAF is fixed at 10 km and at 20 km on the northeast side, consistent with the heat flow and seismicity data. The dip of the fault is prescribed to be vertical, consistent with non-volcanic tremor observed at ~26 km depth along a plane ~1 km NE of the San Andreas Fault along the northern portion of the Carrizo segment which suggests a near-vertical dip of ~88° (Shelly et al., 2009). Values of Young's modulus are set to values representative of the dominate lithologies on each side of the fault, 50 GPa (E_1) southwest of the fault appropriate for granite representing the Salinian block and 75 GPa (E_3) appropriate for sandstones representing the Great Valley Sequence (Stein and Wysession, 2003; Turcotte and Schubert, 2002). The viscosity (η) is set to 3×10^{19} Pa s. Poisson's ratio (ν) is fixed throughout the model to 0.25. The last earthquake on the fault is set to 150 years before the present and out of plane displacements (i.e., the simulated earthquakes) are set to occur every 205 years (Jackson et al., 1995), consistent with the models of Schmalzle et al. (2006). Recent studies suggest that the recurrence interval for the Carrizo Plain may be closer to ~140 ± 46 years (Zielke et al., 2010). Our results, however, are not very sensitive to the assumed recurrence interval, because of the long duration since the last earthquake relative to the value of the relaxation time (viscosity/rigidity) of ~50 years, where the relaxation time represents the duration of time it takes for the visoelastic response of an earthquake to decay away. The models are run through enough earthquake cycles that equilibrium has been reached i.e., it behaves as if an infinite number of earthquakes have occurred. For consistency with the Schmalzle et al. (2006) models, we also allow for 3 mm/yr of movement on the Los Alamos Fault, 60 km southwest of the San Andreas Fault. The variable parameters in the model simulations are the Young's

Please cite this article as: Fulton, P.M., et al., Reconciling patterns of interseismic strain accumulation with thermal observations across the Carrizo segment of the San Andreas Fault, Earth Planet. Sci. Lett. (2010), doi:10.1016/j.epsl.2010.10.024

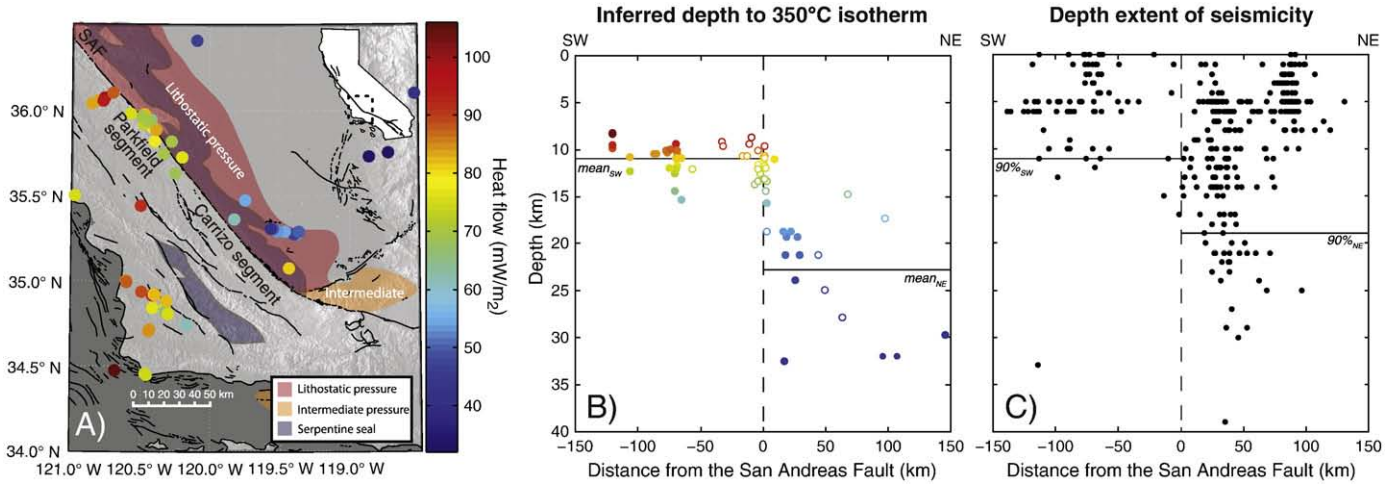

Fig. 2. A) Regional map of the Carrizo and Parkfield segments of the SAF showing locations of heat flow data (points colored by heat flow value) [*USGS California Heat Flow database,* and references therein (http://earthquake.usgs.gov/heatflow/)], the extent of a serpentinite unit associated with the Franciscan Complex interpreted to act as a hydrologic seal (purple shaded regions) (adapted after Irwin, 1990), and regions characterized by intermediate and near-lithostatic overpressures (orange and red shaded regions, respectively) (adapted after Berry, 1973). B) Depth to the brittle ductile transition as a function of distance from SAF. Depths are estimated by using the 350 °C isotherm calculated from the heat flow data for the Carrizo (solid) and Parkfield (open) segments assuming a radiogenic heat production value of 2.0 μW/m^3. Colors are scaled to the corresponding heat flow value. C) Earthquake focal depths from 1975-2009 across the Carrizo segment [*USGS/NEIC database* (http://neic.usgs.gov)]. The 90–95% cutoff depth of seismicity, related to the 350 °C isotherm and the brittle–ductile transition, is shown for each side of the fault. (For interpretation of the references to colour in this figure legend, the reader is referred to the web version of this article.)

modulus of the suspected compliant zone (E_2) and the long-term average slip rate on the San Andreas Fault (R).

3. Results

We run the model for different combinations of fault slip rates and values of Young's Modulus for the compliant zone and use a grid search approach to obtain a low misfit solution based on the χ^2 misfit between the simulated and geodetically observed interseismic velocity field presented by Schmalzle et al. (2006) (Fig. 3). Using the same geodetic data allows us to make comparisons with their models. Our low misfit results yield a slip rate (R) that is identical to the geologically accepted rate ($34^{+1.5}_{-3.0}$ mm/yr) (Sieh and Jahns, 1984), whereas the results of Schmalzle et al. (2006) suggest a geodetic rate of the SAF ~2 mm/yr *faster* than the geologic rate. Interestingly, in order to obtain our low misfit solution, we need a value of E_2 of 30^{+5}_{-10} GPa (Fig. 3C). This result is lower than the estimated value of 40±8 GPa obtained by Schmalzle et al. (2006) and indicates the tradeoff between elastic thicknesses and low rigidity northeast of the fault to satisfy the asymmetry in the geodetic data.

Our low misfit solution ($\chi^2 = 11.51$) provides a statistically similar fit to those obtained by Schmalzle et al. (2006) for a compliant zone and constant elastic thickness ($\chi^2 = 9.30$), and for variable elastic thickness but no compliant zone ($\chi^2 = 10.83$). The similarities of these fits emphasize the non-unique nature of these models. Our new model, however, now honors the heat flow and seismicity data in addition to the geodetic data and geologic slip rate estimate.

4. Discussion

With our values of elastic thickness, the 20 km wide compliant zone NE of the Carrizo segment requires an extremely low value of Young's modulus. Similar contrasts in rigidity have been reported for damage zones associated with major strike-slip faults (Cochran et al., 2009; Fialko, 2004; Fialko et al., 2002; Hamiel and Fialko, 2007). However, a width of 20 km is considerably wider than what would be expected for a damage zone (Vermilye and Scholz, 1998). The width of our inferred compliant zone spatially corresponds with borehole-based geomechanical observations indicating an unusual rotation of the regional stress field (Castillo and Hickman, 1995; Castillo and Younker, 1997) that is suggestive of a laterally extensive compliant zone (e.g., Casey, 1980; Faulkner et al., 2006; Healy, 2008).

Our favored interpretation for the presence of the compliant zone invokes large overpressures at depth that decrease Young's Modulus. This explanation has two facets, first that overpressures (i.e. pore pressures greater than hydrostatic) in this region exist at depth, and second that overpressures can decrease the elastic modulus.

The presence of large overpressures in this region is consistent with the subsurface extent of a hydrologic seal that extends ~10–20 km northeast from the fault throughout much of central California (Irwin, 1990; Irwin and Barnes, 1975) and large overpressures observed in deep wells (Berry, 1973; Castillo and Hickman, 1995; Castillo and Younker, 1997) (Fig. 2). In central California, in situ measurements of pore pressure in deep wells, and values inferred from mud weights used during drilling, suggest the presence of large overpressures at depth northeast of the SAF in marked contrast to hydrostatic values inferred southwest of the fault (Berry, 1973; Castillo and Younker, 1997). Within the compliant zone pore pressures approach lithostatic values (~2.5 times hydrostatic) at depths >~3 km and follow a different trend than similar profiles NE of the compliant zone (Castillo and Younker, 1997). These observations are consistent with numerical modeling results suggesting that large overpressures may develop beneath a regional seal. Fulton and Saffer (2009) suggest that such a seal extends 10–20 km northeast of the SAF, and they illustrate how large overpressures may develop near the fault zone and beneath this regional seal.

Two lines of evidence suggest overpressures can decrease the elastic modulus of rocks. First, overpressures increase crack porosity, which decreases both Young's modulus and Shear modulus (e.g., Dvorkin et al., 1999). Secondly, overpressures inferred from hydrologic observations coupled with numerical models of crustal hydrogeology along the Parkfield segment just north of this area (Berry, 1973; Fulton and Saffer, 2009) are correlated with a wide zone of low seismic velocity (V_p) and high V_p/V_s (Eberhart-Phillips and Michael, 1993; Michelini and McEvilly, 1991). This low velocity zone is interpreted in terms of a reduction in elastic moduli resulting from overpressures (Eberhart-Phillips and Michael, 1993). To our knowledge there is no similar seismic survey across the nearby Carrizo segment of the San Andreas. Intriguingly, however, regional earthquake and ambient noise tomography reveals low velocity structure within a region tens of km wide NE of the fault

Please cite this article as: Fulton, P.M., et al., Reconciling patterns of interseismic strain accumulation with thermal observations across the Carrizo segment of the San Andreas Fault, Earth Planet. Sci. Lett. (2010), doi:10.1016/j.epsl.2010.10.024

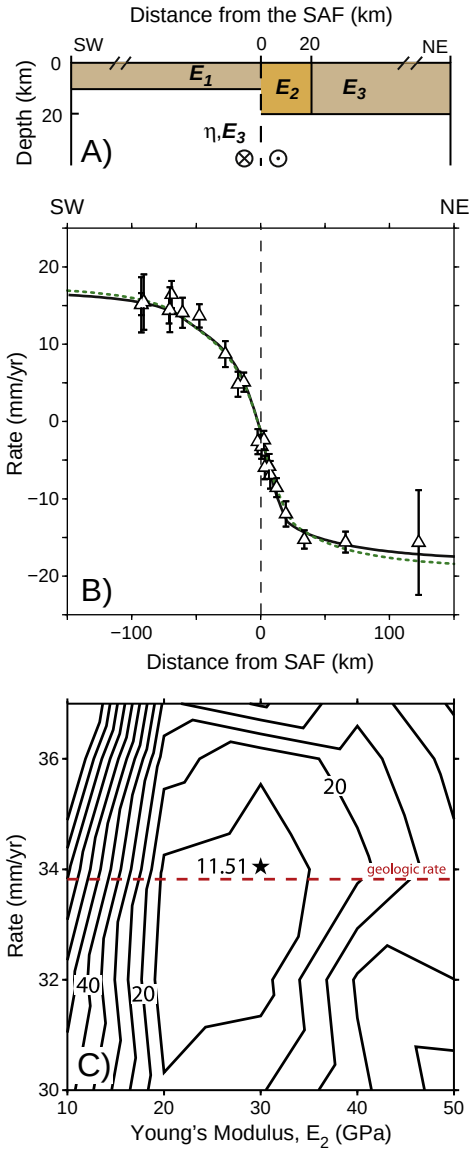

Fig. 3. A) Model domain with contrast in elastic thickness constrained by heat flow and seismicity data. B) Low misfit model result (solid curve; compliant zone Young modulus $E_2 = 30$ GPa and average slip rate $R = 34.1$ mm/yr, consistent with geologically determined rate of 34 mm/yr (Sieh and Jahns, 1984). For comparison, dashed green curve shows the model fit from Schmalzle et al.'s (2006) variable elastic parameters model with constant elastic thickness. C) Contoured values of χ^2 misfit from varying E_2 and R. The geologically determined rate is shown as a red dashed line for comparison. (For interpretation of the references to colour in this figure legend, the reader is referred to the web version of this article.)

along the Carrizo segment that extends to depths throughout much of the crust and suggest a velocity contrast across the fault that may be consistent with our proposed model (Shapiro et al., 2005; Tape et al., 2009).

In addition to overpressures decreasing the elastic moduli, overpressures may also allow for a portion of the excess strain observed within the apparent compliant zone to represent inelastic permanent deformation. This would suggest that in addition to the narrow zone interpreted to be "locked" and supporting large earthquakes, the SAF system in this region may also consist of a wide zone undergoing gradual deformation/creep (<~5 mm/yr accommodated over 20 km) which would not rebound during an earthquake. Although this process is not necessary as part of our interpretation, we note that we cannot exclude it with the interseismic geodetic data alone.

An alternative explanation for the compliant zone is that unusual rocks within the mid to lower crust help contribute to the low Young's Modulus northeast of the fault. Short magnetotelluric profiles across the SAF in central California suggest there is unusual resistive basement northeast of the fault along the Carrizo segment (Mackie et al., 1997; Unsworth et al., 1999). The data have also been interpreted to suggest that there may be less fluid within the fault zone along the Carrizo segment compared with the Parkfield segment (Unsworth et al., 1999). The compliant zone of our model corresponds well to the lateral extent of the Franciscan Complex. Although highly serpentinized rock present in small volumes within the Franciscan may exhibit values of Young's modulus as low as those we interpret (e.g., Glawe and Linard, 2003), we find this explanation unlikely by itself because of the large volume of anomalous material required.

Other explanations for asymmetric strain accumulation, including a dipping fault plane or laterally varying viscosity are unlikely for this region. If a viscosity contrast controlled by lateral differences in subsurface temperature were used to explain the asymmetry, a contrast in heat flow opposite of what is observed would be necessary to explain greater deformation on the northeast side of the fault (e.g., Malservisi et al., 2001). Also, whereas a fault dip of ~60° has been used to explain asymmetric strain accumulation across the San Andreas and San Jacinto faults in southern California (Fialko, 2006), the dip of the fault along the Carrizo segment appears to be vertical to great depth through the crust on the basis of deep tremor locations (e.g., Shelly et al., 2009). Some authors have suggested on the basis of microseismicity, seismic imaging, and potential field studies that the San Andreas Fault dips to the southwest through the Big Bend region to the south and that this southwest dip may continue through the Carrizo segment (Fuis et al., 2008). If so, this would still not be able to explain the geodetic observations; for greater interseismic strain on the northeast side of the fault to result from a dipping fault plane, the fault would have to dip considerably to the northeast rather than to the southwest (Fialko, 2006; Wei and Sandwell, 2008). We suggest that our interpretation of a wide compliant zone northeast of the fault is the most reasonable explanation for the observed asymmetric strain accumulation and an interpretation that is consistent with a wide range of observations.

5. Conclusions

We illustrate that by incorporating thermal and seismicity observations into viscoelastic models of interseismic strain accumulation, we obtain a model that provides greater insight into how interseismic strain accumulates on this "locked" segment of the fault. Our resulting model characterizes the Carrizo segment of the San Andreas Fault with a 10 km thick elastic layer southwest of the fault and a 20 km thick layer northeast of the fault that includes a 20 km wide highly compliant zone situated above a viscous lower crust and upper mantle. This model fits the geodetic data and geologic slip rate well and is consistent with a wide range of independent observations.

An important aspect of this model is that many of the otherwise free parameters are constrained by independent observations. The elastic layer thickness on each side of the fault is constrained by heat flow and seismicity data, the dip of the fault is constrained by the location of deep tremor, and the lateral extent of a possible compliant zone northeast of the fault, interpreted to be ~20 km wide by previous analysis, is consistent with other geologic and geophysical observations. By explicitly including seismicity and thermal data to generate hard constraints on elastic thickness in our model, we are able to make a more robust estimate of Young's modulus in the compliant zone NE of the fault. This value is significantly lower than the previous estimate, and is most simply interpreted in terms of large overpressures. This conclusion has important implications for interpretation of seismic data and is consistent with a number of other observations, including deep well data along the Carrizo segment, and

Please cite this article as: Fulton, P.M., et al., Reconciling patterns of interseismic strain accumulation with thermal observations across the Carrizo segment of the San Andreas Fault, Earth Planet. Sci. Lett. (2010), doi:10.1016/j.epsl.2010.10.024

observations just north along the fault which also suggest that overpressures are reducing the elastic modulus of rocks northeast of the fault. Overall, we show that integrating independent observations helps to better constrain models of geodetic strain, construct reasonable interpretations, and ultimately provides a deeper insight into the underlying processes and properties controlling strain accumulation and seismic hazard.

Acknowledgements

We thank an anonymous reviewer for comments that helped improve this manuscript and Rocco Malservisi for enlightening conversations and Rob Govers for continuing to work on G-TECTON and making it freely available to the scientific community. This project was supported by NSF grant EAR 0545342 to RH and a NASA Earth System Science Fellowship grant (NNG05GA83H) and NSF Earth Science Postdoctoral Fellowship (0847985) to GS.

References

Barbot, S., Fialko, Y., Sandwell, D., 2008. Effect of a compliant fault zone on the inferred earthquake slip distribution. J. Geophys. Res. 113, B06404. doi:10.1029/2007JB005256.

Ben-Zion, Y., Huang, Y., 2002. Dynamic rupture on an interface between a compliant fault zone layer and a stiffer surrounding solid. J. Geophys. Res. 107 (B2), 2042. doi:10.1029/2001JB000254.

Berry, F., 1973. High fluid potentials in California Coast Ranges and their tectonic significance. Am. Assoc. Pet. Geol. Bull. 57, 1219–1249.

Casey, M., 1980. Mechanics of shear zones in isotropic dilatant materials. J. Struct. Geol. 2, 143–147.

Castillo, D., Hickman, S., 1995. Near-field stress and pore pressure observations along the Carrizo Plain segment of the San Andreas fault. EOS Trans. AGU F558 (76), 2005–2012.

Castillo, D.A., Younker, L.W., 1997. A high shear stress segment along the San Andreas Fault: inferences based on near-field stress direction and stress magnitude observations in the Carrizo Plain Area. Lawrence Livermore National Laboratory Technical Report, UCRL-ID-126085 www.osti.gov/servlets/purl/490160-gXk9Xv/webviewable/.

Chéry, J., 2008. Geodetic strain across the San Andreas Fault reflects elastic plate thickness variations (rather than fault slip rate). Earth Planet. Sci. Lett. 269, 352–365.

Cochran, E.S., Li, Y.-G., Shearer, P.M., Barbot, S., Fialko, Y., Vidale, J.E., 2009. Seismic and geodetic evidence for extensive, long-lived fault damage zones. Geology 37, 315–318. doi:10.1130/G25306A.1.

Dvorkin, J., Mavko, G., Nur, A., 1999. Overpressure detection from compressional- and shear-wave data. Geophys. Res. Lett. 26 (22), 3417–3420.

Eberhart-Phillips, D., Michael, A.J., 1993. Three-dimensional velocity structure, seismicity, and fault structure in the Parkfield region, central California. J. Geophys. Res. 98, 15,737–15,758.

Faulkner, D.R., Mitchell, T.M., Healy, D., Heap, M.J., 2006. Slip on 'weak' faults by the rotation of regional stress in the fracture damage zone. Nature 444, 922–925. doi:10.1038/nature05353.

Fay, N.P., Humphreys, E.D., 2005. Fault slip rates, effects of elastic heterogeneity on geodetic data, and the strength of the lower crust in the Salton Trough region, southern California. J. Geophys. Res. 110, B09401. doi:10.1029/2004JB003548.

Fialko, Y., 2004. Probing the mechanical properties of seismically active crust with space geodesy: study of the coseismic deformation due to the 1992 Mw7.3 Landers (southern California) earthquake. J. Geophys. Res. 109, B03307. doi:10.1029/2003JB002756.

Fialko, Y., 2006. Interseismic strain accumulation and the earthquake potential on the southern San Andreas Fault System. Nature 441 (7096), 968–971.

Fialko, Y., Sandwell, D., Agnew, D., Simons, M., Shearer, P., Minster, B., 2002. Deformation on nearby faults induced by the 1999 Hector Mine earthquake. Science 297, 1858–1862.

Fuis, G.S., Scheirer, D.S., Langenheim, V., Kohler, M.D., 2008. The San Andreas Fault in Southern California has a "propeller" shape—implications for tectonics and seismic hazard. Geological Society of America Abstracts with Programs, Vol. 40, No. 6, p. 326.

Fulton, P.M., Saffer, D.M., 2009. Potential role of mantle-derived fluids in weakening the San Andreas Fault. J. Geophys. Res. 114, B07408. doi:10.1029/2008JB006087.

Glawe, U., Linard, J., 2003. High concrete dam on serpentinite. Q. J. Eng. Geol. Hydrogeol. 36 (3), 273–285. doi:10.1144/1470-9236/03-225.

Govers, R., 1993. Dynamics of lithospheric extension; a modeling study, Doctoral thesis. Univ. of Utrecht, Utrecht, Netherlands. 240 pp.

Hamiel, Y., Fialko, Y., 2007. Structure and mechanical properties of faults in the North Anatolian Fault system from InSAR observations of coseismic deformation due to the 1999 Izmit (Turkey) earthquake. J. Geophys. Res. 112, B07412. doi:10.1029/2006JB004777.

Healy, D., 2008. Damage patterns, stress rotations and pore fluid pressures in strike-slip fault zones. J. Geophys. Res. 113, B12407. doi:10.1029/2008JB005655.

Irwin, W.P., 1990. Geology and plate tectonic development. In: Wallace, R.E. (Ed.), The San Andreas Fault System, California: U.S. Geol. Surv. Prof. Pap., 1515, pp. 61–80.

Irwin, W.P., Barnes, I., 1975. Effect of geologic structure and metamorphic fluids on seismic behavior of the San Andreas Fault system in central and northern California. Geology 3, 713–716. doi:10.1130/0091-7613(1975) 3<713:EOGSAM>2.0.CO;2.

Jackson, D.D., Aki, K., Cornell, C.A., Dieterich, J.H., Henyey, T.L., Mahdyiar, M., Schwartz, D., Ward, S.N., 1995. Seismic hazards in southern California—probable earthquakes, 1994 to 2024. Bull. Seismol. Soc. Am. 85, 379–439.

Jolivet, R., Burgmann, R., Houlie, N., 2009. Geodetic exploration of the elastic properties across and within the northern San Andreas Fault zone. Earth Planet. Sci. Lett. 288, 126–131.

Le Pichon, X., Chamot-Rooke, N., Rangin, C., Sengör, A.M.C., 2003. The North Anatolian fault in the Sea of Marmara. J. Geophys. Res. 108 (B4), 2179. doi:10.1029/2002JB001862.

Le Pichon, X., Kreemer, C., Chamot-Rooke, N., 2005. Asymmetry in elastic properties and the evolution of large continental strike-slip faults. J. Geophys. Res. 110, B03405. doi:10.1029/2004JB003343.

Lisowski, M., Savage, J.C., Prescott, W.H., 1991. The velocity-field along the San Andreas Fault in central and southern California. J. Geophys. Res. 96, 8369–8389.

Mackie, R.L., Livelybrooks, D.W., Madden, T.R., Larsen, J.C., 1997. A magnetotelluric investigation of the San Andreas Fault at Carrizo Plain, California. Geophys. Res. Lett. 24 (15), 1847–1850.

Malservisi, R., Furlong, K.P., Dixon, T.H., 2001. Influence of the earthquake cycle and lithospheric rheology on the dynamics of the Eastern California Shear Zone. Geophys. Res. Lett. 28 (14), 2731–2734.

Melosh, H.J., Raefsky, A., 1980. The dynamical origin of subduction zone topography. Geophys. J. R. Astron. Soc. 60, 333–354.

Melosh, H.J., Raefsky, A., 1981. A simple and efficient method for introducing faults into finite element computations. Bull. Seismol. Soc. Am. 71, 1391–1400.

Michelini, A., McEvilly, T.V., 1991. Seismological studies at Parkfield, I. Simultaneous inversion for velocity structure and hypocenters using cubic b-splines parameterization. Bull. Seismol. Soc. Am. 81, 524–552.

Page, B.M., 1981. The Southern Coast Ranges. Prentice-Hall, Upper Saddle River, N. J.

Prescott, W.H., Yu, S.-B., 1986. Geodetic measurement of horizontal deformation in the Northern San Francisco Bay Region, California. J. Geophys. Res. 91 (B7), 7475–7484.

Schmalzle, G., Dixon, T., Malservisi, R., Govers, R., 2006. Strain accumulation across the Carrizo segment of the San Andreas Fault, California: impact of laterally varying crustal properties. J. Geophys. Res. 111, B05403. doi:10.1029/2005JB003843.

Shapiro, N.M., Campillo, M., Stehly, L., Ritzwoller, M.H., 2005. High-resolution surface-wave tomography from ambient seismic noise. Science 307, 1615–1618.

Shelly, D.R., Ellsworth, W.L., Ryberg, T., Haberland, C., Fuis, G.S., Murphy, J., Nadeau, R.M., Bürgmann, R., 2009. Precise location of San Andreas Fault tremors near Cholame, California using seismometer clusters: slip on the deep extension of the fault? Geophys. Res. Lett. 36, L01303. doi:10.1029/2008GL036367.

Sieh, K.E., Jahns, R.H., 1984. Holocene activity of the San Andreas Fault at Wallace Creek, California. Geol. Soc. Am. Bull. 95, 883–896.

Sims, J.D., 1993. Chronology of displacement on the San Andreas Fault in central California: evidence from reversed positions of exotic rock bodies near Parkfield, CA. In: Powell, R.E., Weldon, R.J.I., Matti, J.C. (Eds.), The San Andreas Fault System: Displacement, Palinspastic Reconstruction, and Geologic Evolution: Mem. Geol. Soc. Am., vol. 178, pp. 231–256.

Stein, S., Wysession, M., 2003. An introduction to Seismology, Earthquakes, and Earth Structure, 1st ed. Blackwell, Malden, Mass. 498 pp.

Tape, C., Liu, Q., Maggi, A., Tromp, J., 2009. Adjoint tomography of the Southern California crust. Science 355, 988.

Turcotte, D.L., Schubert, G., 2002. Geodynamics, 2nd Edition. Cambridge University Press, New York. 456 pp.

Unsworth, M., Egbert, G., Booker, J., 1999. High-resolution electromagnetic imaging of the San Andreas fault in Central California. J. Geophys. Res. 104 (B1), 1131–1150.

Vermilye, J., Scholz, C., 1998. The process zone: a microstructural view of fault growth. J. Geophys. Res. 103 (B6), 12223–12237.

Wei, M., Sandwell, D., 2008. Asymmetric velocity across the San Andreas Fault System: the effects of fault dip. Eos Trans. AGU 89 (53) (Fall Meet. Suppl, Abstract S21B-1828).

Zielke, O., Arrowsmith, J.R., Grant Ludwig, L., Akçiz, S.O., 2010. Slip in the 1857 and earlier large earthquakes along the Carrizo Plain, San Andreas Fault. Science. doi:10.1126/science.1182781.

Please cite this article as: Fulton, P.M., et al., Reconciling patterns of interseismic strain accumulation with thermal observations across the Carrizo segment of the San Andreas Fault, Earth Planet. Sci. Lett. (2010), doi:10.1016/j.epsl.2010.10.024